A Molecular Mechanism for Non-Photochemical Quenching in Cyanobacteria

Yue Lu[1,2], **Haijun Liu**[2,3], **Rafael Saer**[2,3], **Veronica L. Li**[1,2], **Hao Zhang**[1,2], **Liuqing Shi**[1], **Carrie Goodson**[2,3], **Michael L. Gross**[1,2], and **Robert E. Blankenship**[1,2,3]

[1]Department of Chemistry, Washington University in St. Louis, St. Louis, MO 63130, USA

[2]Photosynthetic Antenna Research Center, Washington University in St. Louis, St. Louis, Missouri 63130, USA

[3]Department of Biology, Washington University in St. Louis, St. Louis, MO 63130, USA

Abstract

The cyanobacterial Orange Carotenoid Protein (OCP) protects photosynthetic cyanobacteria from photodamage by dissipating excess excitation energy collected by phycobilisomes (PBS) as heat. Dissociation of the PBS-OCP complex *in vivo* is facilitated by another protein known as the Fluorescence Recovery Protein (FRP), which primarily exists as a dimeric complex. We used various mass spectrometry(MS)-based techniques to investigate the molecular mechanism of this FRP-mediated process. FRP in the dimeric state (dFRP) retains its high affinity to the C-terminal domain (CTD) of OCP in the red state (OCP^r). Site-directed mutagenesis and native MS suggest the head region on FRP is a binding candidate to OCP. After attachment to the CTD, the conformational changes of dFRP enable dFRP to bridge the two domains, facilitating the reversion of OCP^r into the orange state (OCP^o) accompanied by a structural rearrangement of dFRP. Interestingly, we found a mutual response between FRP and OCP; that is, FRP and OCP^r destabilize each other, whereas FRP and OCP^o stabilize each other. A detailed mechanism of FRP function is proposed on the basis of the experimental results.
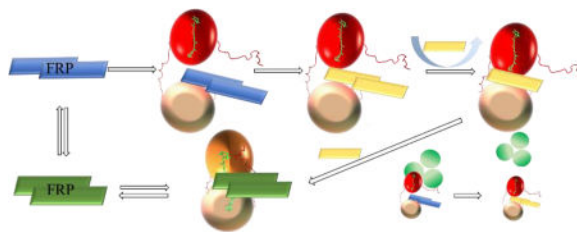
For Table of Contents Use Only

Introduction

Solar energy is utilized by photosynthetic organisms to produce and store chemical energy, later to be used to power cellular processes. Excess light energy is detrimental, however, to photosynthetic organism, resulting in oxidative stress, and ultimately leading to the damage of photosynthetic apparatus or even the death of the cell. Light-regulation strategies, therefore, are necessary for balancing the absorption and utilization of light energy. One of the most important protection mechanisms is called non-photochemical quenching (NPQ), during which excited-state chlorophylls or other pigments are quenched, and excess excitation energy is dissipated as heat[1]. In plants and algae, NPQ is carried out by light-harvesting antennas, a process mediated by a pH gradient across the thylakoid membrane. NPQ is also related to the xanthophyll cycle, which plays an important role in the protection of plants and algae against oxidative stress[1, 2]. Unlike the integral membrane light-harvesting complexes in plants and algae, a distinct photo-protection mechanism has evolved in cyanobacteria. This protection utilizes a major, soluble light-harvesting complex, called the phycobilisome (PBS), which is attached to the surface of the membrane. An orange carotenoid protein (OCP), a single carotenoid-binding protein, interacts with the PBS and functions both as a light sensor and a photoprotective entity[3–7].

The OCP is composed of an α-helical N-terminal domain (NTD), an α-helix/β-sheet C-terminal domain (CTD), and a flexible linker that joins them. A keto-carotenoid spans both domains and is encapsulated by the protein scaffold with almost no solvent exposure[5, 8]. The OCP forms a compact globular structure by a strong interaction between the NTD and CTD via salt bridges and hydrogen bonds. Under high-intensity light illumination, these bonds are broken, leading to the solvent exposure of the major NTD-CTD interface, accompanied by a 12 Å carotenoid translocation. This process converts orange OCP (OCP^o) into its active quenching (red) state (OCP^r) [8–14]. It is generally accepted that OCP^r quenches energy and fluorescence via its interaction with the core of the PBS. Efforts have been made to locate the specific binding site on PBS, and several models were proposed[15–19]. FRP is able to recover the fluorescence from the PBS by interacting with OCP^r. The active OCP^r is metastable, and reverts back to the inactive orange state in the dark. FRP greatly accelerates this reversion process by interacting with the CTD[20, 21]. The FRP crystal structure reveals three conformational states: two in a dimeric form and one in a tetrameric form. The dimeric form was proposed to be the functional state[21], and it is the dominant state in solution[21–23]. A study of the OCP apo protein suggests FRP functions as a general scaffold protein for OCP maturation[14]. The recent model proposed by Thurotte et al.[24] indicates that FRP has two distinct activities during the fluorescence recovery process: it first accelerates OCP^r detachment from phycobilisomes[25] and then assists OCP^r relaxation into OCP^o.

Nevertheless, the detailed molecular mechanism of how FRP mediates the fluorescence recovery process in cyanobacteria remains elusive.

We chose mass spectrometry (MS) to investigate this problem. MS is now being widely used to study protein conformation, structure, dynamics, and protein-protein or protein-ligand interactions[26–30]. Native MS, in particular, allows for the detection and analysis of intact protein complexes in their near-native states[31, 32]. Cross-linking complements native MS because it can reveal amino acid pairs that are positioned in close proximity by linking the protein partners via those residues as constrained by an effective length of the linker[33]. A medium-resolution interaction model can be obtained by mapping the adjacent residues on protein complexes[28]. MS-based isotope-encoded cross-linking can provide quantitative information on protein interactions, giving insights into the binding sites as well as conformation changes[34]. Further, MS-based protein footprinting techniques can afford detailed information on protein solvent accessibility[35–38]. All in all, we show that an integrative MS-based tool kit can provide complementary information of protein structures in complexes to afford a more complete description of an interaction model.

In this work, we utilized a variety of approaches, particularly MS-based ones, to investigate the molecular mechanism of the FRP-mediated OCP^r to OCP^o conversion process. We found that FRP accelerates OCP^r to OCP^o conversion through several distinct steps. A dramatic conformational change of FRP occurs upon interacting with OCP in both the red and orange states. In addition, the head domain on FRP may play an essential role during its binding to OCP. Our study provides novel insights into the FRP-mediated OCP^r to OCP^o process and allows us to propose a working model based on the experimental results.

Materials and Methods

Expression and mutagenesis of FRP

The expression of WT FRP (SGL_RS10235) was performed as previously reported[22]. Site-directed mutants of FRP were constructed by using complementary mutagenic PCR primers. A list of all the primers used is shown in Table S1. Each mutagenic PCR reaction consisted of ~50 ng of plasmid DNA, 10 pmol of each primer, 10 nmol of dNTPs, 0.5 μL of a high-fidelity DNA polymerase (Phusion, Thermo Fisher Scientific, Waltham MA), and 10 μL of a 5x PCR reaction buffer (Phusion HF buffer, Thermo Fisher Scientific) in a 50 μL of solution. The PCR reaction consisted of an initial denaturation step at 98 °C for 15 sec, followed by 18 cycles of 98 °C for 15 sec, 50 °C for 20 sec, and 72 °C for 20 sec. Because the length of the SGL_RS10235 gene is short, a final extension step was not included in the PCR reaction. Following the mutagenic PCR reaction, 1 μL of DpnI restriction enzyme (New England Biolabs, Ipswich, MA) was added to each reaction to digest the original template DNA. Five microliters of this reaction were used to transform chemically competent *E. coli* DH10B cells. Plasmids extracted from the transformants were confirmed by DNA sequencing prior to a subsequent transformation of the closed circular plasmid into *E. Coli* BL21(DE3) cells for protein expression.

FRP and OCP purification

The isolation of OCP, FRP and FRP mutants was performed by using published protocols[19, 22]. The OCP[r] partial digestion was carried out as previously described[39].

Native MS and IM-MS Analysis of NTD, CTD and FRP complex

The NTD/CTD mixture obtained after OCP[r] partial digestion and FRP samples were separately washed with 400 mM ammonium acetate at pH = 8.0 (09689, Sigma-Aldrich, Missouri, USA) in a 5 kDa molecular weight cut off filter (Vivaspin, Goettingen, Germany). The original buffer and salts were removed by 10 cycles of washing. The NTD/CTD and FRP were mixed in 4:1 and 1:4 ratios, respectively, and introduced into the ESI source of a Waters Synapt G2 ESI Q-TOF (Electrospray ionization-quadrupole time of flight, Waters Corporation, Milford, MA) mass spectrometer by using commercial borosilicate emitters with extra coating (ES387, Hudson, New Hampshire, Thermo Scientific). The backing pressure was adjusted to 5 mBar for transferring the large protein ions. All the mutant FRP proteins were mixed with the NTD/CTD in a 2:1 ratio, respectively, and analyzed in the same manner. As a reference, intact OCP was also mixed with FRP in a 1:2 ratio to investigate the affinity of FRP to OCP[o]. The IM-MS experiment and data processing were carried out as previously described[22].

Activity assays

The OCP was previously photoconverted to the red form by 10 min illumination with 2,000 μmol photons $m^{-2}s^{-1}$ white light at 8 °C. The OCP[r] to OCP[o] reversion processes in the absence/presence of FRP WT/mutants were monitored in a Lambda 950 (Perkin Elmer UV WinLab) spectrophotometer at 8 °C. One point was recorded per second by monitoring the absorption at 550 nm for 30 min.

Cross-linking and LC-MS

All the cross-linking experiments were carried out in triplicate at 4 °C for 2 h. Illumination with 2,000 μmol photons $m^{-2}s^{-1}$ white light was kept constant during the cross-linking process for OCP[r]-included samples. The cross-linker, disuccinimidyl suberate (DSS-d_0, cross-linking reagent without any deuterium atoms, ProteoChem, UT, USA), was added to FRP (reference 1), OCP[o] and OCP[r]-FRP samples. DSS-d_4 (cross-linking reagent with four deuterium atoms, to provide a 4 Dalton mas shift for encoding purposes, ProteoChem, UT, USA) was added to FRP (reference 2), OCP[r] and OCP[o]-FRP samples. OCP[r]-FRP[d4] and OCP[o]-FRP[d0]; FRP[d4], OCP[o, d4] and OCP[o]-FRP[d0]; FRP[d0], OCP[r, d0] and OCP[r]-FRP[d4] were mixed, respectively, in equimolar quantities to investigate the structural changes and interacting regions of these proteins. (See Fig. S1 for a flow chart). The molecular weight of cross-linked complexes was analyzed by SDS-PAGE. After crosslinking, the proteins were isolated by acetone precipitation and digested with trypsin(??) as previously described[40]. Sep Pak cartridges (Waters Corporation, Milford, MA) were used to desalt the peptide sample. The peptides were analyzed with an LC-MS experiment, as previously described, with some adjustments[41]. Peptide mixtures were trapped by a guard column (nanoACQUITY Trap Column, Waters Corporation, Milford, MA) and then fractionated on an ACQUITY UPLC Peptide BEH C18 Column (10 K psi, 130 Å, 1.7 μm, 75 μm × 100

mm, Waters Corporation, Milford, MA). The MS analysis was performed with a Thermo Scientific™ Q Exactive™ hybrid quadrupole-Orbitrap mass spectrometer (Thermo Fisher Scientific, Bremen Germany). Peptides were eluted with a 120 min, 250 nL/min gradient coupled to the nanospray source. The default charge state was 3, and the scan range was from m/z 380–1500. Mass spectra were obtained at high mass resolving power (70,000, FWHM at m/z 200), and the top 15 most abundant ions corresponding to eluting peptides per scan were submitted to collision-induced dissociation (CID) in the ion trap, with charge-state rejection of unassigned, +1, +2 and >+8 ions enabled. Precursor ions were added to a dynamic exclusion list for 8 s to ensure a good sampling of each elution peak.

GEE Labeling

The FRP protein was mixed with OCP^r and OCP^o in a 2:1 ratio. The modification reaction was carried out for up to 2 h under either dark or light conditions at 4 °C, using freshly prepared 1.5 M GEE (Sigma, St. Louis, MO) and 0.5 M EDC (Pierce, Rockford, IL) stock solutions (10 mM PBS, pH 8.0). The reaction was quenched by adding a 1/10 volume of 1 M Tris–HCl (pH 8.0) followed by buffer-exchange using a Zeba™ desalting spin column (Thermo Scientific, Rockford, IL) according to the manufacture's protocol. The FRP-only sample was also labeled by GEE on the same platform as the control. Preparing the peptides and conducting the LC/MS experiments were performed in the same way as for the cross-linked samples[42].

MS data analysis

Byonics[43] and Protein Prospector online server (Baker, P.R. and Clauser, K.R. http://prospector.ucsf.edu) were utilized to identify DSS- and GEE-labeled peptides. The search parameters were set as follows: peptide tolerance: 10 ppm; MS/MS tolerance: 0.02 Da; mass type: monoisotopic; ^{13}C isotope ions: yes; enzyme: trypsin; missed cleavages: 2.

Results and Discussion

FPR accelerates OCP^r to OCP^o relaxation by bridging NTD and CTD

The OCP is a unique protein that functions as a light sensor, a signal propagator, and an energy quencher. The NTD is a chromophore-containing domain that can burrow into the PBS and thermally dissipate excess excitation energy, whereas the CTD can regulate the accessibility of OCP and, hence, the activity of the PBS-binding NTD[18, 44, 45]. The spontaneous reversion from the red to the orange state of OCP is significantly accelerated in the presence of FRP[21, 25, 46]. Under light irradiation, the most exposed cleavage sites for trypsin are located on the linker region of OCP owing to complete domain dissociation[12]. Thus, fragments of the CTD (186–310) and NTD (10–170) can be obtained by partial proteolysis, whereas parts of the linker region and N-terminal arm (flexible loop region located on the N- termini) are not formed[39]. Immunoprecipitation, size-exclusion chromatography (SEC), native-gel electrophoresis, and molecular modelling all suggest that the CTD is the domain that interacts with FRP[16, 21, 47]. Our previous native MS study shows that FRP primarily exists as a dimer[22], although two different oligomeric states were identified by crystallography[21].

In this study, we mixed FRP with NTD/CTD partial digestion fragments in 4:1 and 1:4 ratios and subjected them to native MS analysis. The electrospray ionized protein complex in the gas phase carries a series of charges that usually exhibit a Gaussian-like distribution. We were able to make peak assignments both manually and by using Massign software[48]. The results indicate that a highly abundant dFRP-CTD complex is formed (Fig.1), offering convincing evidence of the high affinity of the CTD to dFRP[48]. Collisional induced dissociation (CID) of this protein complex produces monomeric FRP-CTD (mFRP), suggesting a strong interaction between one FRP monomer and the CTD (Fig. 2A). A previous ion mobility(IM)-MS analysis shows one intermediate state in the unfolding process of dFRP[22], and none in the unfolding of the CTD owing to its compact structure[39]. Here, two intermediate states occur during the unfolding of CTD-dFRP, driven by the higher order structure refolding, suggesting high stability of this complex (Fig. S2).

Surprisingly, we observed with native MS that protein complexes containing components of the NTD, dFRP, and CTD co-exist with the CTD-dFRP complex. NTD fragments (sequences from 10–168 and 10–170 with and without carotenoid, respectively) are binding partners to the dFRP-CTD (Fig. 1A). We then carried out tandem MS to investigate the topology of those protein complexes. Accelerating protein complex ions to high kinetic energy usually results in ejection of a single protein subunit[49]. After ejection, complexes including the dFRP-NTD and mFRP-NTD remain, giving evidence for the existence of a binding face between FRP and the NTD (Fig. 2B). Interestingly, no such complexes were detected by an MS1 analysis, when no MS/MS activation was applied. The previous study on FRP and NTD mixture also shows FRP doesn't bind to NTD[47]. It appears that the binding of the CTD to dFRP initiates a conformational change of dFRP, facilitating its binding to the NTD. In other words, the determining step of OCP^r binding to dFRP event is the attachment of CTD to dFRP. An interface between CTD and NTD might also exist in the protein complex CTD-dFRP-NTD, but the interaction is likely to be weak because we found no NTD-CTD complex with or without CID.

We also observed the formation of complexes consisting of the dCTD-dFRP-NTD and dCTD-dFRP (Fig. 1). To investigate whether the CTD can form a dimer by itself, the NTD/CTD, we submitted the mixture to native MS at concentrations ranging from 5 μM to 200 μM. The analysis revealed a noticeable level of dimeric CTD (dCTD), even at low concentrations (Fig. S3), which is in accord with the previous SEC results[47]. Thus, our results show formation of a complex of dCTD-dFRP, owing to the binding of dCTD to dFRP. These results suggest that different regions of the CTD are involved in binding to the other CTD and FRP. Similarly, the NTD could bind to this dCTD-dFRP complex forming dCTD-dFRP-NTD. When the NTD/CTD is in excess, more dCTD-dFRP-NTD complexes are formed (Fig. 1B).

To describe better the interaction between FRP and OCP, we adopted an isotopic cross-linking strategy to compare quantitatively their interactions under dark or illuminated conditions[34]. Although isotope encoding is commonly used to facilitate identification of crosslinks, we are using it here to make quantitative comparisons. SDS-PAGE analysis revealed bands corresponding to the molecular weights of one FRP and one OCP and two FRPs and one OCP in the red state, whereas the corresponding bands in the orange state

were barely visible (Fig. S4). It appears that mFRP-OCP is more abundant than dFRP-OCP on the gel image, but we don't see that as a direct evidence of dFRP monomerization. Usually only a very small fraction of interacting protein complex can be cross-linked. To find dFRP-OCP, mFRP needs to be cross-linked to the other mFRP and OCP needs to be cross-linked to mFRP, which lowers the chance of obtaining them. Nevertheless, among all the lysine-NH_2 groups in OCP (twelve) and FRP (eight), and the N-termini of the two proteins, we identified by LC/MS six cross-links (Fig. 3A). We found a residue located at the CTD (K249) to be linked to K23 on FRP, further proving that the CTD is adjacent to the FRP. In addition, the linker region and the N-terminal arm of OCP are cross-linked to FRP (Fig. 3A, product-ion (MS/MS) spectra are shown in Fig. S5). Mapping the cross-linked residues on the FRP and OCP crystal structures reveals that the cross-linked residues are located near the interface of two terminal domains (Fig. 3B, C, D).

Mutant proteins reveal critical residues in binding of FRP to CTD

To locate the binding site of FRP, we generated a series of FRP site-directed mutants based on conservation analysis[21] and analyzed them with the same native MS platform. That the spray produced both FRP, NTD/CTD, and complexes is direct evidence of the binding affinity between mutant FRP and the NTD/CTD. The charging (+11, +12 and +13) for the dFRP-CTD complex decreased for all mutant samples; that is, to +9 and +10 for the two mutants mentioned above (Fig. 4C and Fig. S6A). The F76D mutant exhibits the most striking decrease in interaction, as determined for the relative abundances of the complexes, and the binding of the K102D mutant to the NTD/CTD is also severely affected. Overlapping the three crystallographic conformations[21] shows that FRP is composed conservatively of an extended α-helical domain, a small helical cap, whereas the chain regions are folded differently. F76 and K102 are located on the conserved helical cap ("head" region) in all three conformations (Fig. S7A). Based on the affinity analysis of CTD to dFRP, we propose that this head domain is the binding face of FRP to the CTD. The certainty of this assignment can be increased by more experiments (e.g., construction of different mutations on the head region).

CTD shows a negatively charged interface that is hidden in the orange state (Fig. S8A, B), whereas the binding domain of FRP is positively charged (Fig. 5A, B). In previous mutagenesis studies on OCP, the "catalytic" ability of FRP was found to be greatly affected by the mutations on the surface charge of the inter-domain cavity[51]. One explanation is that the positively charged head domain of FRP interacts with the negatively charged interface on the CTD. In addition, the other side of the head, which is originally embedded between the head and an FRP chain, is negatively charged (Fig. 5D, F). The NTD interface that is hidden in the orange state has a positively charged surface (Fig. S8C, D). One possibility is that, upon binding of the positively charged head domain of FRP to the negatively charged CTD interface, the head domain on FRP unfolds, exposing the originally embedded negative face that interacts with the positively charged interface on the NTD. In brief, one conclusion of the molecular modelling and surface electrostatic analysis is OCP and FRP interact via an unfolding and bridging mechanism. After the head domain attaches to the CTD, the head domain unfolds and the original hidden face on the head domain attaches to the NTD.

Rate measurements reveal regions influencing FRP function

To evaluate the residues that influence the function of FRP, and not just its binding affinity, we performed a kinetic analysis of the OCP^r to OCP^o relaxation process by monitoring changes in the absorption at 550 nm in the presence of different FRP mutants. The F76D and R60L mutants lose their ability to accelerate OCP^r conversion, and the G65D mutation also greatly affects the FRP function (Fig. 6). A previous study also demonstrates that the R60L mutant loses its acceleration ability on OCP^r relaxation[21]. The result with the F76D mutant is not surprising, as this mutant loses its affinity to interact with the NTD/CTD, as discussed in the previous section. The R60L mutant can still bind to the NTD/CTD to some degree (Fig. S6E), although no acceleration capability on OCP^r relaxation is retained (Fig. 6). We propose that the binding and the acceleration of OCP^r relaxation processes can be decoupled because different amino acids are involved. Native MS provides a snapshot of the interaction between the FRP and OCP^r (without the linker region and N-terminal arm), whereas the kinetic analysis is of the FRP performing its function by converting OCP^r into OCP^o. R60 is not located in the binding face on FRP; thus, the binding affinity of FRP is not affected by substitution of this residue. Thurotte and co-workers[24] found that the R60L mutant can still detach OCP from the PBS, but it is unable to accelerate the conversion to the orange state. Both results indicate that the acceleration process can be decoupled into several stages. In addition, the R60L mutant FRP can still undergo a conformation change upon binding with the CTD, as the dFRP-CTD-NTD complex was also observed during native MS analysis (data not shown). It is likely that R60 is the crucial residue in the later conformational change, when the two domains are already attaching to FRP.

Substantial conformational changes of dFRP occur upon bridging the two domains

To investigate the possible conformational changes that take place upon bringing the two domains together, we utilized intra-molecular cross-links on FRP to evaluate the structural change upon its interaction with OCP. When FRP interacts with OCP^r, the intensity of intra-molecular links increase several fold, whereas the signal intensity for the intra-molecular cross-link intensity decreases when FRP is incubated with OCP^o (Fig. 7). The cross-links identified here can either arise from one individual chain, or two subunits of dFRP, although the abundance of cross-linked dFRP is much lower than intra-linked mFRP, as observed by SDS-PAGE (Fig. S4). The measured distance of the cross-linked amino acid pairs within chains A/C, B/D, and E/F, as well as dimeric AC, BD and EF (Fig. S7B) are listed in Table S2. Although the spacer length of DSS is 11.4 Å, a distance constraint of 26–30 Å between Cα atoms is considered to be possible owing to native-state protein dynamics[52]. AC and BD dimers have a higher chance to form intra-molecular links than the EF dimer when considering the distance constraints. Nevertheless, a substantial structural rearrangement of FRP takes place upon interaction with OCP, especially when OCP is in the red state.

Interestingly, we identified cross-links between two mFRP subunits: M1 to M1 and K23 to K23. We also found an increased number of M1-M1 cross-links when FRP interacts with OCP^r and, and a decreased number when FRP interacts with OCP^o (Fig. S9B). In addition, the frequency of K23-K23 cross-linking also drops when FRP interacts with OCP^o compared to when it interacts with OCP^r (Fig. S9B). One explanation is the flexible N-terminal loops on each mFRP approach each other when dFRP interacts with OCP^r, and not

when dFRP interacts with OCP^o; the regions containing K23 on each mFRP move apart. when dFRP interacts with OCP^o. Another possibility is that FRP becomes more dynamic when performing its function accelerating the OCP^r to OCP^o conversion and, thus, has a larger chance to be cross-linked; when FRP interacts with OCP^o, the dynamics of FRP are restricted, disfavoring formation of inter-mFRP links.

GEE footprinting of carboxyl groups probes solvent accessibility changes of FRP

To investigate further the conformational change of FRP upon interaction with OCP, we probed the solvent accessibility of the protein by evaluating the intensity change of DSS mono-links and GEE-labeled residues in a carboxyl (GEE) footprinting experiment. When FRP interacts with OCP^r, the signals for all the mono-links show an increased intensity except that for K99, which is located on the binding domain of FRP (Fig. 4D). To get a more comprehensive or higher resolution picture of solvent accessibility under various conditions, we adopted GEE footprinting to follow the carboxyl groups on the amino-acid residues. The reactivity of GEE and a carboxyl group on D and E amino-acid side chains is proportionally related to its solvent-accessible surface area and that of regions adjoining D and E[38].

Similar to that of most of the lysine residues, the solvent accessibility of all the D and E residues of FRP increase dramatically upon interacting with OCP^r (Fig. 4E), supporting the idea that FRP undergoes a dramatic conformational change during its interaction with OCP^r. The most dramatic change is for D54, followed by those for D68 and D69 (Fig. 4E). The mutagenesis analysis shows that the amino acids (R60, W50 and D54)that form a network of hydrogen bonds between the two mFRP chains are essential for the enhancement of OCP^r to OCP^o conversion[21]. In addition, three previous studies suggest that FRP monomerizes when interacting with OCP analogs[14, 23, 53]. In this study, we saw a protein complex including mFRP, CTD and NTD after MS/MS dissociation (Fig. 2B). Thus, the dramatic solvent accessibility change on D54 may be caused by a structural rearrangement of two FRP subunits—perhaps via a monomerization of dFRP. The increased amount of inter-mFRP M1-M1 cross-links, however, contradicts the monomerization idea of dFRP during its interaction with OCP^r. It is worth mentioning that OCP^r is under constant illumination at low temperature during the footprinting, and the samples including OCP^r still exhibit a red color upon quenching of the reaction. Thus, the FRP has not reached the end of its journey to convert the OCP^r into the orange form. After dFRP attaches to the two domains, the departing mFRP may be in equilibrium with both the bound mFRP and free mFRP in solution (Fig. 3C). It is likely that increased dynamics facilitate forming of inter-mFRP and intra-FRP cross-links (Fig. 7, Fig. S9B). Another possibility is FRP unfolds into a long alpha helix, increasing the solvent accessibility. In this new conformation, the N-termini of each mFRP come closer than in the original structure.

Crosslinking shows the response of OCP^r to FRP

In this part of the study, we identified multiple cross-links between OCP^r-K167, -K170, and -P2 to FRP, suggesting that the N-terminal arm and linker region are adjoining during the interaction with FRP (Fig. 3). In addition, both domains can attach to FRP, despite the CTD being the major target of FRP, as discussed in the previous section. The two domains of OCP move away from each other upon photoactivation, whereas an unstructured loop (the linker

region) connecting the two domains becomes significantly exposed[12]. That the OCP photo-activation is not reversible after partial enzymatic digestion indicates that this unstructured loop is crucial for the conversion of active OCP[r] to inactive OCP[o]. The N-terminal arm is also a crucial coordinator in the OCP conversion process; this arm not only move away from the CTD but becomes disordered during the activation[12, 42]. Moreover, the absence of the N-terminal arm largely facilitates the action of FRP on OCP[r] and accelerates the detachment of the OCP[r] from the PBS[54]. Those previously published findings reinforce our conclusion that the linker-region, N-terminal arm, and CTD on OCP[r] may be adjacent to the regions that are interacting with FRP.

The extents of both DSS mono-linking and GEE-labeling on OCP[r] are not generally different in the presence or absence of FRP. An exception is residue E311, which is located at the C-terminal loop of OCP (Fig. 3D); its decrease in solvent accessibility suggests it could be an important binding residue to FRP (Fig. 8A). The C-terminal loop of OCP is not fully seen in the crystal structures, owing likely to its flexibility[8, 9]. Our previous GEE-labeling study shows, upon photoactivation, a marked increase in the extent of E311 labeling[42] as well as a > 2-fold decrease in the labeling of P309/K310 in OCP[r] relative to that of the corresponding amino acids in OCP[o] [12]. Both results suggest a movement or structural rearrangement of the C-terminus upon photoactivation. In this study, we found that the C-terminal loop plays a role in the FRP-mediated OCP[r] to OCP[o] conversion process. In addition, that the FRP burrows into the inter-cavity of the two OCP domains may separate them further, exposing the linker region to a larger extent (increased mono-crosslink labeling extent on K167) and slightly increasing the solvent accessibility of K249 on the CTD interface (Fig. 8C).

Crosslinking reveals the response of OCP[o] to FRP

That FRP (in excess) prevents OCP[o] from photoactivation[23, 46] suggests two possible mechanisms: one is that FRP associates with OCP[o] and hinders its activation, and the other is that FRP immediately converts OCP[r] to OCP[o], precluding the detection of OCP[r]. OCP[o] was proposed to be weakly or not attached at all to FRP by an immuno-precipitation study[46], and a similar study on the NTD/CTD reveals that only the CTD can bind FRP[21]. The results obtained by Sluchanko et al.[23] suggest a transient interaction between FRP and OCP[o]. In this study, we confirmed the interaction between FRP and OCP[o], and found that the linker region adjoins FRP during the interaction.

We found a cross-link between the linker region and FRP. Unlike for OCP[r], only one cross-link between OCP[o] and FRP could be identified (Fig. 8D). The intensity of the signal representing this cross-link is much lower compared to that for the red state, suggesting a much smaller interface or binding affinity. The only residues exhibiting a noticeable decrease of solvent accessibility upon binding to FRP are D35 (from GEE labeling) and T15 (from DSS cross-linking) (Fig. 8B, C). These results suggest that the NTD of the orange state associates with the FRP to some degree.

In addition, the signal intensities representing intra-molecular links on FRP all decreased when interacting with OCP[o] (Fig. 7). This could be due to the anchoring of dFRP on OCP[o], slowing dynamics, or the transitions into other states of FRP. In addition, the formation of

OCP-dFRP is barely detectable by native MS (Fig. S10), and the corresponding bands on SDS-PAGE are barely visible (Fig. S4). Thus, the interaction between OCP^o and FRP is significantly weaker than that of OCP^r and FRP.

Conclusion

We propose that FRP performs its function through several independent steps involving various amino-acid residues based on experimental results, though further research is necessary to prove this model. The accelerated conversion process starts with dFRP binding to the CTD on OCP^r, as suggested by native MS results. Those results and others from site-directed mutagenesis (F76, K102), and the mono-crosslink at K99 point to the CTD as the initial binding domain on FRP. The structural rearrangement of dFRP upon binding with the CTD enables its binding to the NTD. To the best of our knowledge, this is the first experimental evidence showing the interaction between the NTD on OCP^r and dFRP. Considering the cross-links found between two domains of OCP and FRP, we propose a bridging mechanism, which is in accord with previous molecular modeling[16]. In that model, the CTD interacts with both head and chain domains of the FRP, whereas the NTD is in contact only with the head domain.

We also propose here that the head domain interacts with the two domains of OCP, explaining the low affinity of OCP^o to FRP; that is, the binding face is hidden owing to the compact structure of the orange state. Furthermore, a previous publication suggests the N-terminal arm on OCP interferes with the interaction with FRP[49]. Our cross-linking results suggest the N-terminal arm adjoins FRP, reinforcing this view. To reset OCP^r to its compact structure, the FRP interaction must bring the two domains together, preparing for the translocation of carotenoid. Native MS provide the direct evidence that NTD, CTD and dFRP can form a stable complex.

The cross-linking results also suggest the interface on NTD and CTD adjoins FRP. Monomerization of either dFRP causes unfolding into a long alpha helix after dFRP bridges the two domains, enabled by the crucial role of residue R60 in this conformational change. The linker region or N-terminal arm of OCP may be crucial in inducing the structural rearrangement of dFRP. [12]In the orange state, the linker region is associated with dFRP to a lesser degree, and the NTD also may retain affinity to dFRP (Fig. 9). In addition, we found an interesting mutual response between FRP and OCP. FRP destabilizes OCP^r by accelerating its conversion to the orange state, whereas FRP itself is also "destabilized". FRP can "lock" OCP^o in the orange state, while FRP itself is also "stabilized" by OCP^o. Thus, we propose that when FRP interacts with OCP^o, a "stiff" structure forms, whereas when FRP interacts with OCP^r, a more dynamic structure is produced.[21]

This study offers new insights into the interaction between FRP and OCP, laying the groundwork for further investigations into the energy-transfer regulation mechanisms of cyanobacterial NPQ.

Supplementary Material

Refer to Web version on PubMed Central for supplementary material.

Acknowledgments

References

1. Niyogi KK, Truong TB. Evolution of flexible non-photochemical quenching mechanisms that regulate light harvesting in oxygenic photosynthesis. Curr. Opin. Plant Biol. 2013; 16:307–314. [PubMed: 23583332]

2. Latowski D, Kuczy ska P, Strzałka K. Xanthophyll cycle – a mechanism protecting plants against oxidative stress. Redox Rep. 2011; 16:78–90. [PubMed: 21722416]

3. Kirilovsky D, Kerfeld CA. Cyanobacterial photoprotection by the orange carotenoid protein. Nat. Plants. 2016; 2:16180. [PubMed: 27909300]

4. Kirilovsky D. Modulating energy arriving at photochemical reaction centers: orange carotenoid protein-related photoprotection and state transitions. Photosynth. Res. 2015; 126:3–17. [PubMed: 25139327]

5. Wilson A, Ajlani G, Verbavatz J-M, Vass I, Kerfeld CA, Kirilovsky D. A Soluble Carotenoid Protein Involved in Phycobilisome-Related Energy Dissipation in Cyanobacteria. Plant cell. 2006; 18:992–1007. [PubMed: 16531492]

6. Bao H, Melnicki MR, Kerfeld CA. Structure and functions of Orange Carotenoid Protein homologs in cyanobacteria. Curr. Opin. Plant Biol. 2017; 37:1–9. [PubMed: 28391046]

7. Kirilovsky D, Kerfeld CA. The orange carotenoid protein in photoprotection of photosystem II in cyanobacteria. Biochim. Biophys. Acta. – Bioenergetics. 2012; 1817:158–166.

8. Kerfeld CA, Sawaya MR, Brahmandam V, Cascio D, Ho KK, Trevithick-Sutton CC, Krogmann DW, Yeates TO. The Crystal Structure of a Cyanobacterial Water-Soluble Carotenoid Binding Protein. Structure. 2003; 11:55–65. [PubMed: 12517340]

9. Wilson A, Kinney JN, Zwart PH, Punginelli C, D'Haene S, Perreau F, Klein MG, Kirilovsky D, Kerfeld CA. Structural Determinants Underlying Photoprotection in the Photoactive Orange Carotenoid Protein of Cyanobacteria. J. Biol. Chem. 2010; 285:18364–18375. [PubMed: 20368334]

10. Kirilovsky D. Photoprotection in cyanobacteria: the orange carotenoid protein (OCP)-related non-photochemical-quenching mechanism. Photosynth. Res. 2007; 93:7. [PubMed: 17486426]

11. Leverenz RL, Sutter M, Wilson A, Gupta S, Thurotte A, Bourcier de Carbon C, Petzold CJ, Ralston C, Perreau F, Kirilovsky D, Kerfeld CA. A 12 Å carotenoid translocation in a photoswitch associated with cyanobacterial photoprotection. Science. 2015; 348:1463–1466. [PubMed: 26113721]

12. Gupta S, Guttman M, Leverenz RL, Zhumadilova K, Pawlowski EG, Petzold CJ, Lee KK, Ralston CY, Kerfeld CA. Local and global structural drivers for the photoactivation of the orange carotenoid protein. Proc. Natl. Acad. Sci. U.S.A. 2015; 112:E5567–E5574. [PubMed: 26385969]

13. Maksimov EG, Sluchanko NN, Mironov KS, Shirshin EA, Klementiev KE, Tsoraev GV, Moldenhauer M, Friedrich T, Los DA, Allakhverdiev SI, Paschenko VZ, Rubin AB. Fluorescent Labeling Preserving OCP Photoactivity Reveals Its Reorganization during the Photocycle. Biophys. J. 2017; 112:46–56. [PubMed: 28076815]

14. Moldenhauer M, Sluchanko NN, Tavraz NN, Junghans C, Buhrke D, Willoweit M, Chiappisi L, Schmitt F-J, Vukojevi V, Shirshin EA, Ponomarev VY, Paschenko VZ, Gradzielski M, Maksimov EG, Friedrich T. Interaction of the signaling state analog and the apoprotein form of the orange carotenoid protein with the fluorescence recovery protein. Photosynth. Res. 2017:1–15.

15. Stadnichuk IN, Krasilnikov PM, Zlenko DV, Freidzon AY, Yanyushin MF, Rubin AB. Electronic coupling of the phycobilisome with the orange carotenoid protein and fluorescence quenching. Photosynth. Res. 2015; 124:315–335. [PubMed: 25948498]

16. Zlenko DV, Krasilnikov PM, Stadnichuk IN. Role of inter-domain cavity in the attachment of the orange carotenoid protein to the phycobilisome core and to the fluorescence recovery protein. J. Biomol. Struct. Dyn. 2016; 34:486–496. [PubMed: 25905572]

17. Blankenship, RE. Molecular Mechanisms of Photosynthesis. Wiley; 2002.

18. Harris D, Tal O, Jallet D, Wilson A, Kirilovsky D, Adir N. Orange carotenoid protein burrows into the phycobilisome to provide photoprotection. Proc. Natl. Acad. Sci. U.S.A. 2016; 113:E1655–E1662. [PubMed: 26957606]

19. Zhang H, Liu H, Niedzwiedzki DM, Prado M, Jiang J, Gross ML, Blankenship RE. Molecular Mechanism of Photoactivation and Structural Location of the Cyanobacterial Orange Carotenoid Protein. Biochemistry. 2014; 53:13–19. [PubMed: 24359496]

20. Gwizdala M, Wilson A, Omairi-Nasser A, Kirilovsky D. Characterization of the Synechocystis PCC 6803 Fluorescence Recovery Protein involved in photoprotection. Biochim. Biophys. Acta. - Bioenergetics. 2013; 1827:348–354.

21. Sutter M, Wilson A, Leverenz RL, Lopez-Igual R, Thurotte A, Salmeen AE, Kirilovsky D, Kerfeld CA. Crystal structure of the FRP and identification of the active site for modulation of OCP-mediated photoprotection in cyanobacteria. Proc. Natl. Acad. Sci. U.S.A. 2013; 110:10022–10027. [PubMed: 23716688]

22. Lu Y, Liu H, Saer RG, Zhang H, Meyer CM, Li VL, Shi L, King JD, Gross ML, Blankenship RE. Native Mass Spectrometry Analysis of Oligomerization States of Fluorescence Recovery Protein and Orange Carotenoid Protein: Two Proteins Involved in the Cyanobacterial Photoprotection Cycle. Biochemistry. 2017; 56:160–166. [PubMed: 27997134]

23. Sluchanko NN, Klementiev KE, Shirshin EA, Tsoraev GV, Friedrich T, Maksimov EG. The purple Trp288Ala mutant of Synechocystis OCP persistently quenches phycobilisome fluorescence and tightly interacts with FRP. Biochim. Biophys. Acta. – Bioenergetics. 2017; 1858:1–11.

24. Thurotte A, de Carbon CB, Wilson A, Talbot L, Cot S, López-Igual R, Kirilovsky D. The cyanobacterial Fluorescence Recovery Protein has two distinct activities: Orange Carotenoid Protein amino acids involved in FRP interaction. Biochim. Biophys. Acta. – Bioenergetics. 2017; 1858:308–317.

25. Gwizdala M, Wilson A, Kirilovsky D. In Vitro Reconstitution of the Cyanobacterial Photoprotective Mechanism Mediated by the Orange Carotenoid Protein in Synechocystis PCC 6803. Plant cell. 2011; 23:2631–2643. [PubMed: 21764991]

26. Marcoux J, Robinson Carol V. Twenty Years of Gas Phase Structural Biology. Structure. 2013; 21:1541–1550. [PubMed: 24010713]

27. Walzthoeni T, Leitner A, Stengel F, Aebersold R. Mass spectrometry supported determination of protein complex structure. Curr. Opin. Plant Biol. 2013; 23:252–260.

28. Rappsilber J. The beginning of a beautiful friendship: Cross-linking/mass spectrometry and modelling of proteins and multi-protein complexes. J. Struct. Biol. 2011; 173:530–540. [PubMed: 21029779]

29. Konermann L, Tong X, Pan Y. Protein structure and dynamics studied by mass spectrometry: H/D exchange, hydroxyl radical labeling, and related approaches. J. Mass Spectrom. 2008; 43:1021–1036. [PubMed: 18523973]

30. Sharon M, Robinson CV. The Role of Mass Spectrometry in Structure Elucidation of Dynamic Protein Complexes. Annu. Rev. Biochem. 2007; 76:167–193. [PubMed: 17328674]

31. Zhang H, Cui W, Gross ML, Blankenship RE. Native mass spectrometry of photosynthetic pigment-protein complexes. FEBS Lett. 2013; 587:1012–1020. [PubMed: 23337874]

32. Boeri Erba E, Petosa C. The emerging role of native mass spectrometry in characterizing the structure and dynamics of macromolecular complexes. Protein Sci. 2015; 24:1176–1192. [PubMed: 25676284]

33. Bullock JMA, Schwab J, Thalassinos K, Topf M. The Importance of Non-accessible Crosslinks and Solvent Accessible Surface Distance in Modeling Proteins with Restraints From Crosslinking Mass Spectrometry. Mol. Cell. Proteomics. 2016; 15:2491–2500. [PubMed: 27150526]

34. Schmidt C, Robinson CV. A comparative cross-linking strategy to probe conformational changes in protein complexes. Nat. Protocols. 2014; 9:2224–2236. [PubMed: 25144272]

35. Zhang H, Cui W, Gross ML. Mass spectrometry for the biophysical characterization of therapeutic monoclonal antibodies. FEBS Lett. 2014; 588:308–317. [PubMed: 24291257]

36. Maleknia SD, Downard KM. Advances in radical probe mass spectrometry for protein footprinting in chemical biology applications. Chem. Soc. Rev. 2014; 43:3244–3258. [PubMed: 24590115]

37. Schermann SM, Simmons DA, Konermann L. Mass spectrometry-based approaches to protein-ligand interactions. Expert Rev. Proteomics. 2005; 2:475–485. [PubMed: 16097882]

38. Zhang H, Wen J, Huang RYC, Blankenship RE, Gross ML. Mass spectrometry-based carboxyl footprinting of proteins: method evaluation. Int. J. Mass Spectrom. 2012; 312:78–86. [PubMed: 22408386]

39. Zhang H, Liu H, Lu Y, Wolf NR, Gross ML, Blankenship RE. Native Mass Spectrometry and Ion Mobility Characterize the Orange Carotenoid Protein Functional Domains. hBiochim. Biophys. Acta. – Bioenergetics. 2016

40. Liu H, Zhang H, Orf GS, Lu Y, Jiang J, King JD, Wolf NR, Gross ML, Blankenship RE. Dramatic Domain Rearrangements of the Cyanobacterial Orange Carotenoid Protein upon Photoactivation. Biochemistry. 2016; 55:1003–1009. [PubMed: 26848988]

41. Lu Y, Zhang H, Niedzwiedzki DM, Jiang J, Blankenship RE, Gross ML. Fast Photochemical Oxidation of Proteins Maps the Topology of Intrinsic Membrane Proteins: Light-Harvesting Complex 2 in a Nanodisc. Anal. Chem. 2016; 88:8827–8834. [PubMed: 27500903]

42. Liu H, Zhang H, King JD, Wolf NR, Prado M, Gross ML, Blankenship RE. Mass spectrometry footprinting reveals the structural rearrangements of cyanobacterial orange carotenoid protein upon light activation. Biochim. Biophys. Acta. – Bioenergetics. 2014; 1837:1955–1963.

43. Bern M, Kil YJ, Becker C. Byonic: Advanced Peptide and Protein Identification Software. Curr. Protoc. Bioinformatics. 2012; 13 13.20.

44. Leverenz RL, Jallet D, Li MD, Mathies RA, Kirilovsky D, Kerfeld CA. Structural and functional modularity of the orange carotenoid protein: distinct roles for the N- and C-terminal domains in cyanobacterial photoprotection. Plant cell. 2014; 26:426–437. [PubMed: 24399299]

45. Kirilovsky D, Kerfeld CA. The Orange Carotenoid Protein: a blue-green light photoactive protein. Photochem. Photobiol. Sci. 2013; 12:1135–1143. [PubMed: 23396391]

46. Boulay C, Wilson A, D'Haene S, Kirilovsky D. Identification of a protein required for recovery of full antenna capacity in OCP-related photoprotective mechanism in cyanobacteria. Proc. Natl. Acad. Sci. U.S.A. 2010; 107:11620–11625. [PubMed: 20534537]

47. Moldenhauer M, Sluchanko NN, Buhrke D, Zlenko DV, Tavraz NN, Schmitt F-J, Hildebrandt P, Maksimov EG, Friedrich T. Assembly of photoactive Orange Carotenoid Protein from its domains unravels a carotenoid shuttle mechanism. Photosynth. Res. 2017:1–15.

48. Morgner N, Robinson CV. Massign: An Assignment Strategy for Maximizing Information from the Mass Spectra of Heterogeneous Protein Assemblies. Anal. Chem. 2012; 84:2939–2948. [PubMed: 22409725]

49. Popa V, Trecroce DA, McAllister RG, Konermann L. Collision-Induced Dissociation of Electrosprayed Protein Complexes: An All-Atom Molecular Dynamics Model with Mobile Protons. J. Phys. Chem. B. 2016; 120:5114–5124. [PubMed: 27218677]

50. Goddard TD, Huang CC, Ferrin TE. Visualizing density maps with UCSF Chimera. J. Struct. Biol. 2007; 157:281–287. [PubMed: 16963278]

51. Wilson A, Gwizdala M, Mezzetti A, Alexandre M, Kerfeld CA, Kirilovsky D. The Essential Role of the N-Terminal Domain of the Orange Carotenoid Protein in Cyanobacterial Photoprotection: Importance of a Positive Charge for Phycobilisome Binding. Plant cell. 2012; 24:1972–1983. [PubMed: 22634762]

52. Merkley ED, Rysavy S, Kahraman A, Hafen RP, Daggett V, Adkins JN. Distance restraints from crosslinking mass spectrometry: Mining a molecular dynamics simulation database to evaluate lysine-lysine distances. Protein Sci. 2014; 23:747–759. [PubMed: 24639379]

53. Shirshin EA, Nikonova EE, Kuzminov FI, Sluchanko NN, Elanskaya IV, Gorbunov MY, Fadeev VV, Friedrich T, Maksimov EG. Biophysical modeling of in vitro and in vivo processes underlying regulated photoprotective mechanism in cyanobacteria. Photosynth. Res. 2017:1–11.
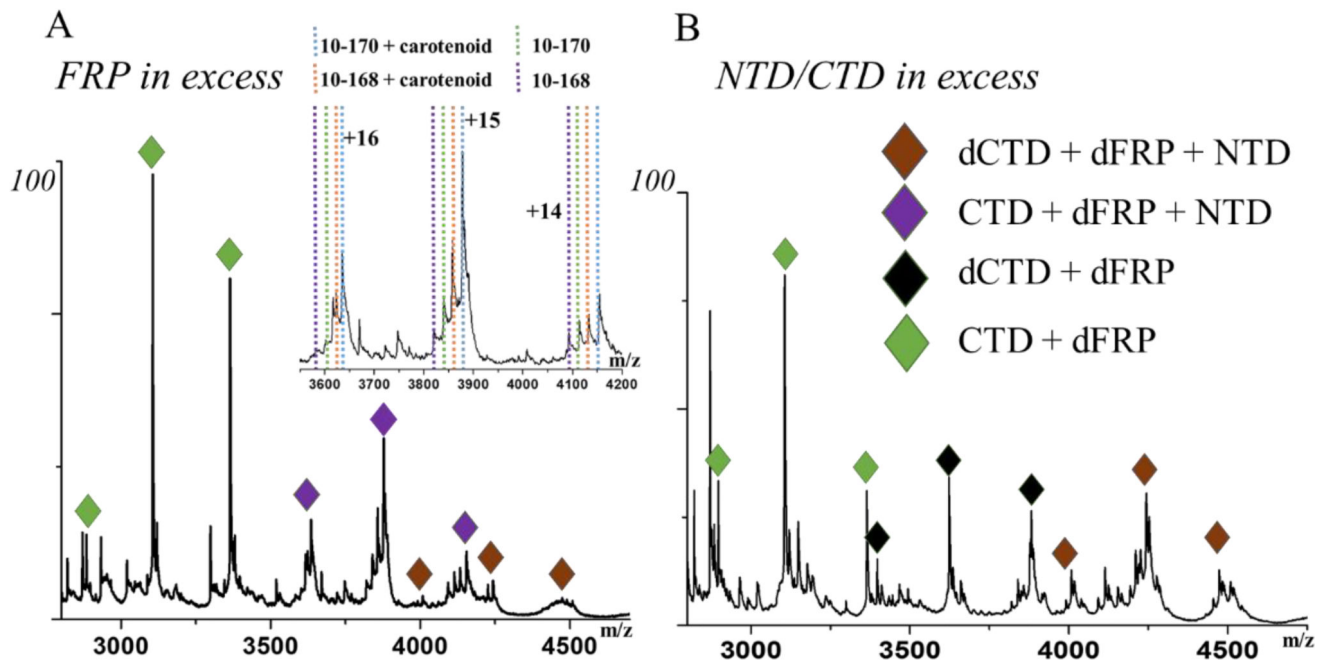
54. Thurotte A, Lopez Igual R, Wilson A, Comolet L, Bourcier de Carbon C, Xiao F, Kirilovsky D. Regulation of Orange Carotenoid Protein activity in cyanobacterial photoprotection. Plant Physiol. 2015; 169:734–747.
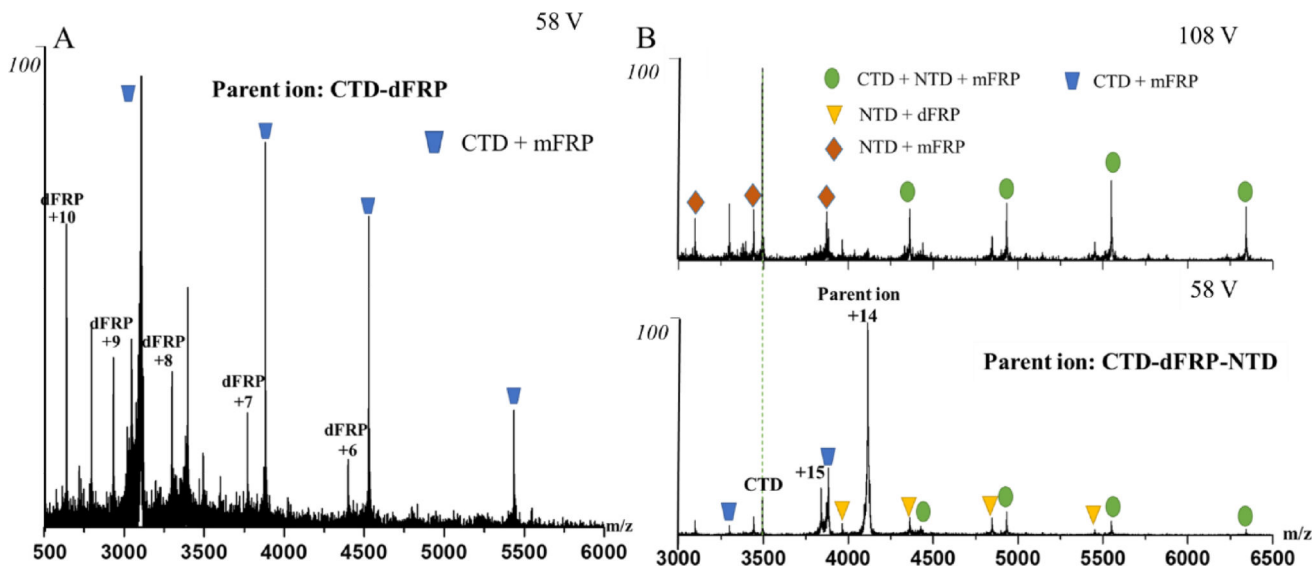
Fig. 1.
Native mass spectra of FRP and the NTD/CTD mixture in a (A) 4:1 or (B) 1:4 ratio.
Complexes include the dCTD-dFRP-NTD, CTD-dFRP-NTD, dCTD-dFRP and CTD-dFRP.
The inset in A shows the binding of the NTD fragments to the dFRP-CTD.

Fig. 2.
(A) Product-ion (MS/MS) spectrum of the CTD-dFRP ion obtained at 58 V collision voltage. The resolved complex of the CTD-mFRP suggests a primary binding face exists on one of the FRP subunits. (B) Product-ion (MS/MS) spectra of CTD-dFRP-NTD recorded at 58 V and 108 V collisional voltage. The resolved complexes of NTD-dFRP and NTD-mFRP after CID suggest that a binding interface exists between the NTD and FRP.
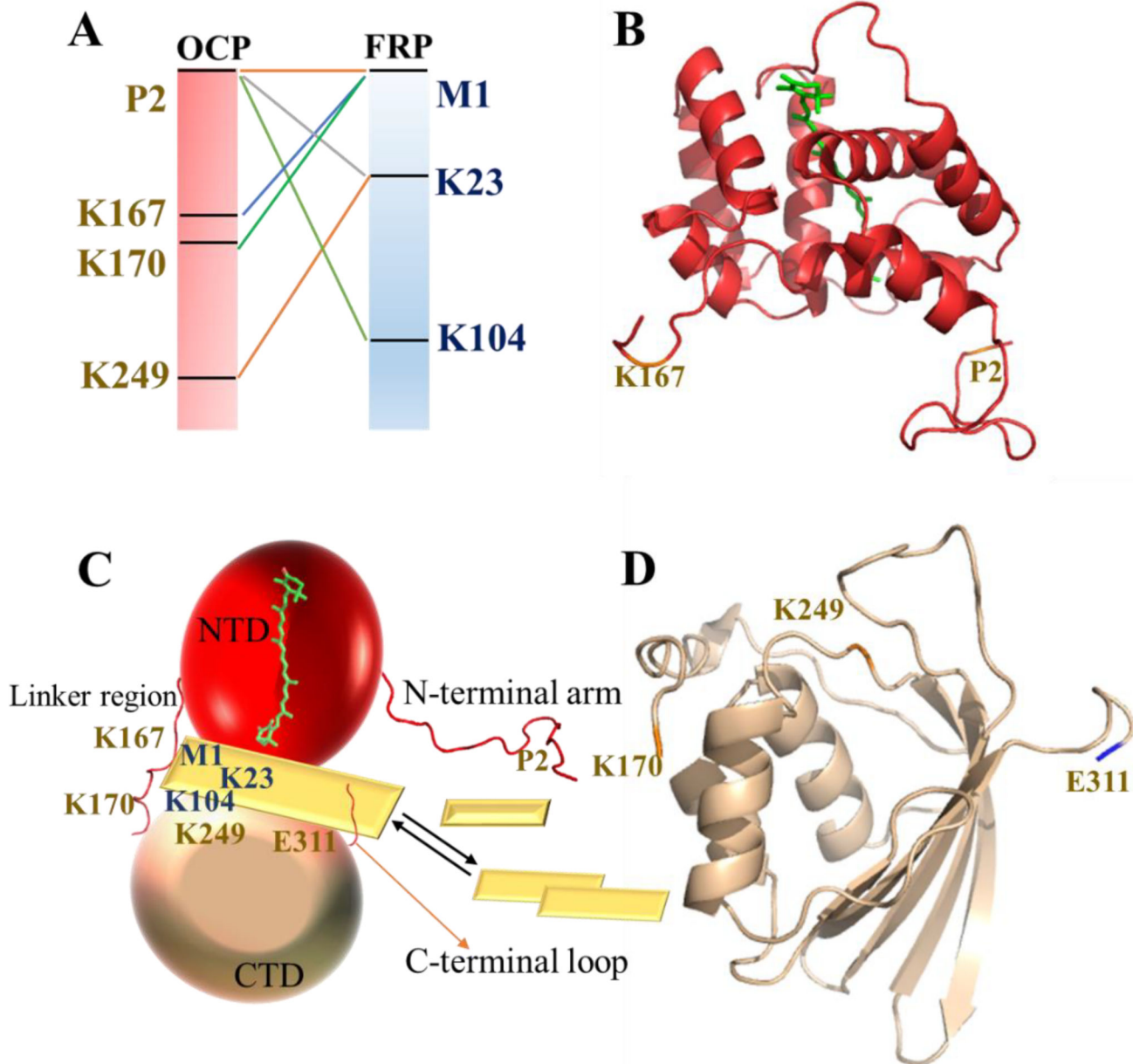
Fig. 3.
(A) Cross-links identified between OCP[r] and FRP. The corresponding positions are mapped on the cartoon representations of the OCP NTD (B, PDB 4XB5[11]) and CTD (D, PDB 3MG1[9], sequence 170–311) crystal structures. (C) Model of the OCP-FRP interaction from crosslinking data. The missing loop regions in the crystal structure were generated by software available at UCSF[50]. Each mFRP unit is shown by a yellow rhombus.
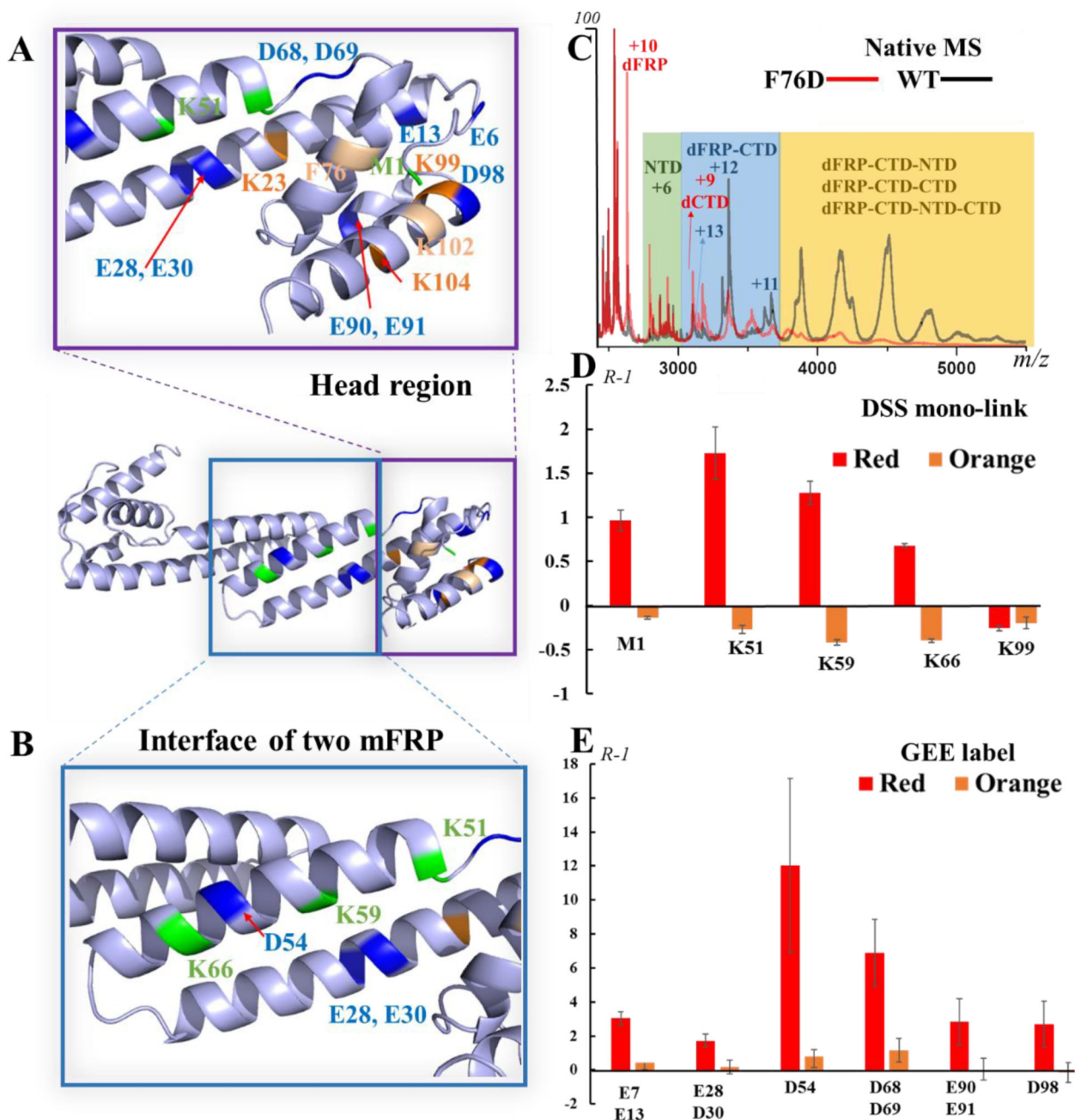
Fig. 4.

Map of residues identified by native MS, cross-linking, and GEE labeling on the FRP head region (A) and dimer-interacting region (B) of chains B/D; structure from PDB 4JDX.[21] (C) Native mass spectra of the NTD/CTD in the presence of WT or F76D FRP. The binding affinity of F76D mutant to NTD/CTD is greatly diminished. (D) A bar graph showing the changing of mono-link extent on FRP in the presence of OCP^r or OCP^o.

$$R = \frac{\text{Abudance of FRP monolink upon FRP interacting with OCP}}{\text{Abudance of FRP monolink for FRP only sample}}$$

(E) Bar graph showing the change in solvent accessibility of FRP residues, as probed by GEE labeling.
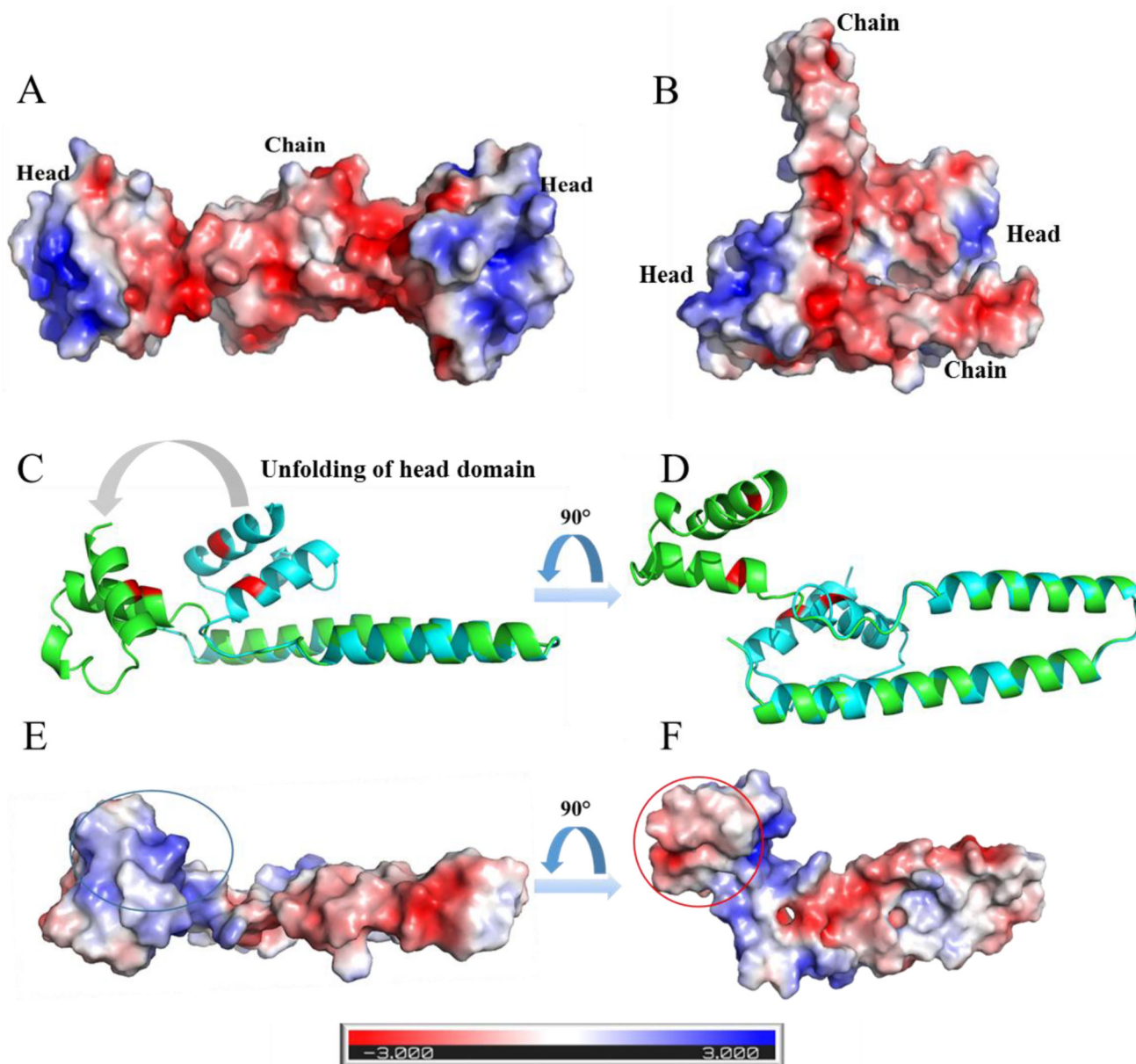
Fig. 5.
The surface electrostatic analysis by APBS shows negatively charged head domains and positively charged chain domain of BD (A) and AC (B) dimer from PDB 4JDX. Chain B (cyan) is aligned to the "unfolded" chain B (Green) as shown in C and D, and the corresponding surface electrostatic analysis of the "unfolded" chain B are shown in E and F. The positively charged binding region is highlighted with blue circle, and the negatively charged region, which in hidden in original state, is highlighted with red circle. The modified structure of chain B (Green) was generated by using the structure building and energy minimization tools in Chimera software[50]. The dihedral angles in the loop region from AA 68–73 (DDRQSV) were modified. Then the produced geometry was energy
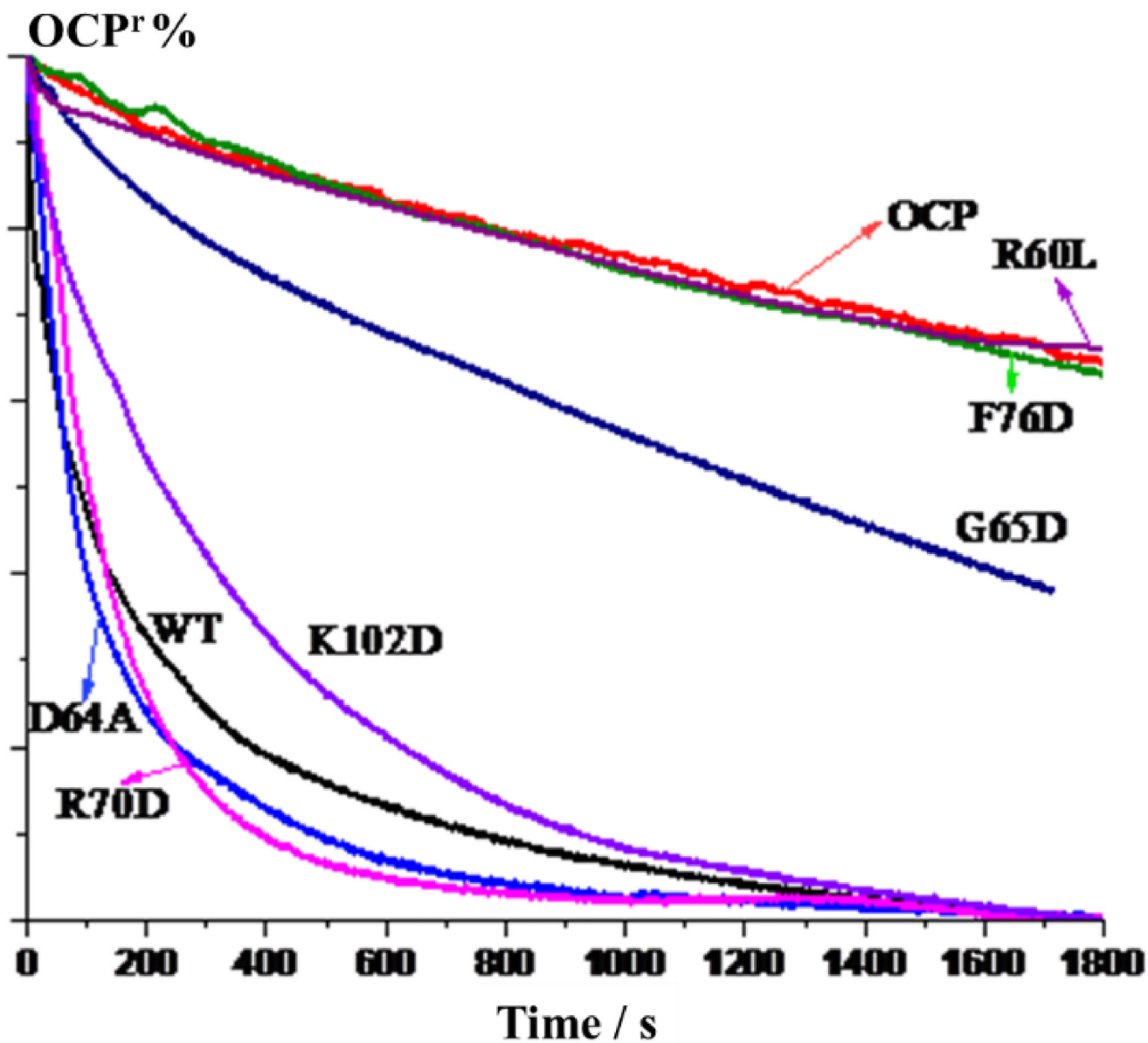
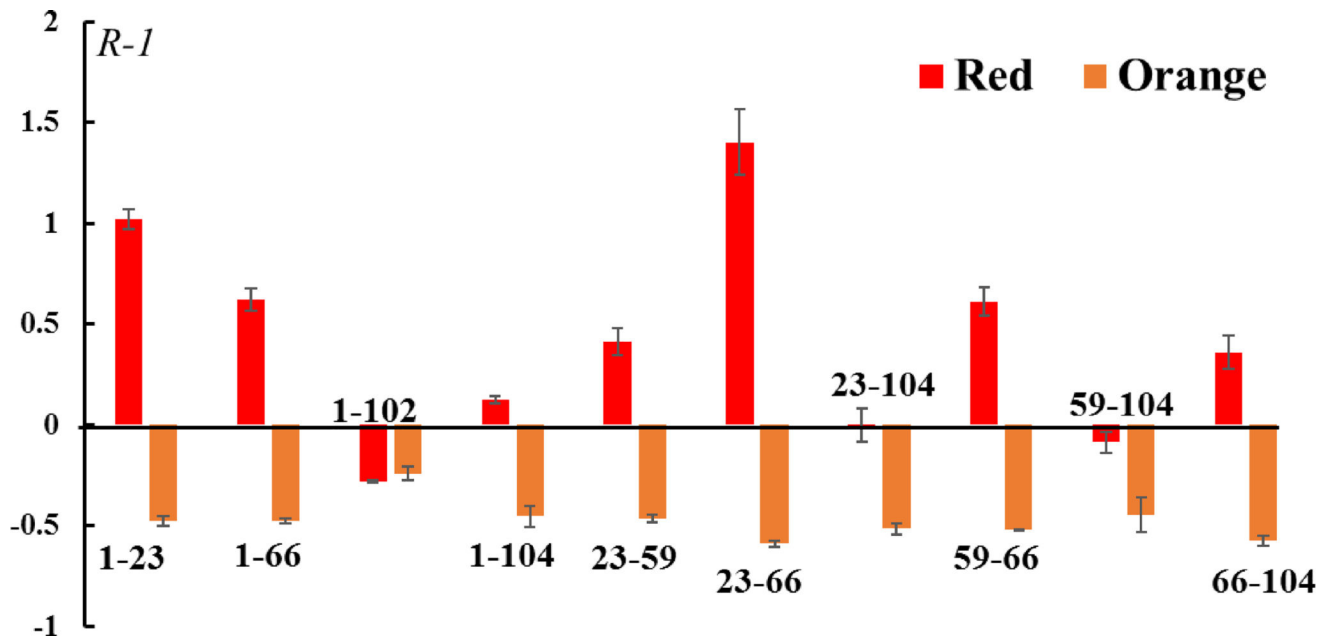minimized by applying 1000 steepest descent steps with a step size of 0.02 angstrom (C, D, E, F).

Fig. 6.
Kinetics of the conversion of OCP^r to OCP^o as monitored by changes of the 550 nm absorption. OCP was either incubated alone, in the presence of WT FRP, or with the FRP mutants R70D, D64A, K102D, G65D, F76D, R60L.

Fig. 7.
Bar graph showing the changes in intra-FRP cross-links in the presence of OCP^r or OCP^o.
The numbers on x axis correspond to the position of amino acid residues on FRP.

$$R = \frac{\text{Abudance of intra} - \text{FRP crosslink upon FRP interacting with OCP}}{\text{Abudance of intra} - \text{Frp crosslink for FRP only sample}}$$
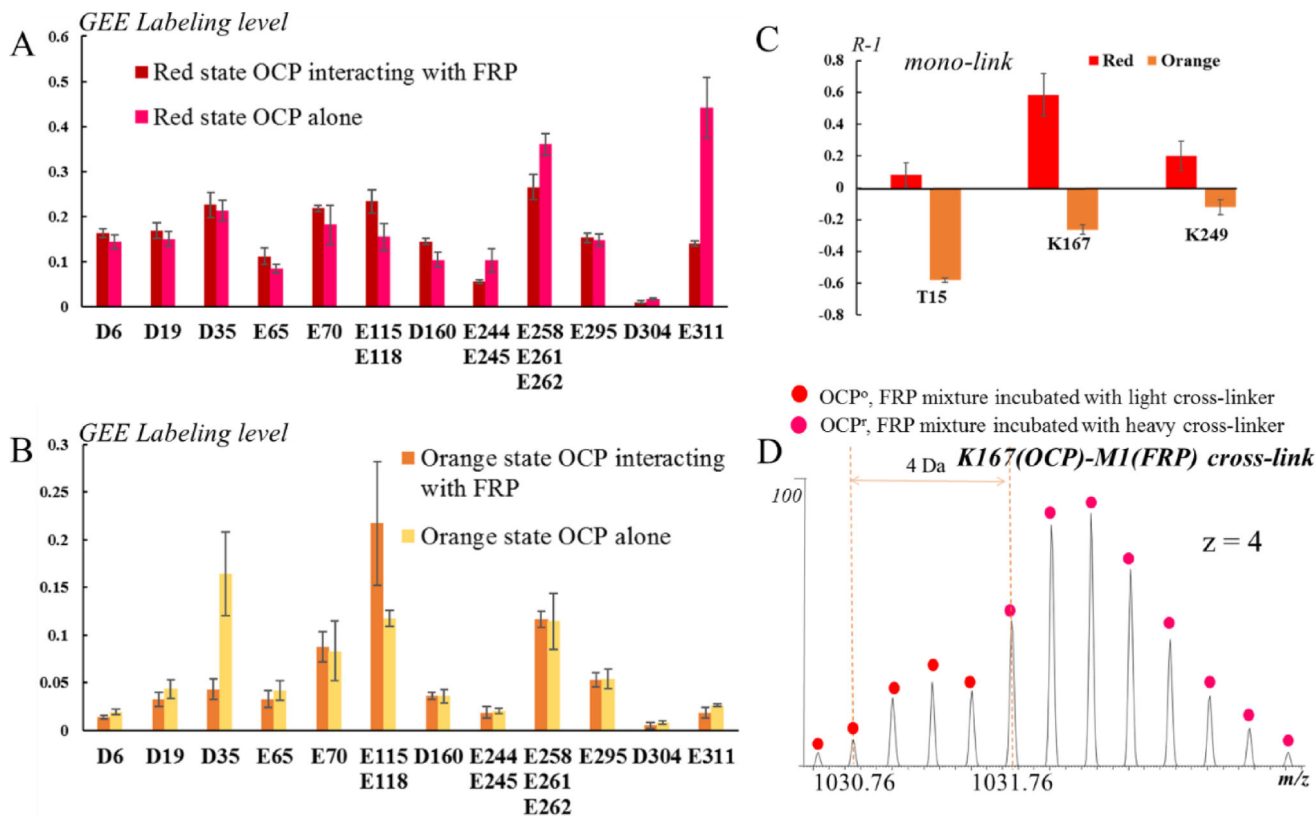
Fig. 8.

(A) GEE labeling extents of OCP^r amino-acid residues in the presence or absence of FRP.

(B) GEE labeling level of OCP^o amino acid residues in the presence or absence of FRP.

$$\text{GEE labeling level} = \frac{\text{Peak area of labled peptide}}{\text{Peak area of labled peptide} + \text{Peak area of unlabled peptide}}$$

(C) A bar graph showing the changes in OCP mono-links in the presence FRP.

$$R = \frac{\text{Abudance of monolink upon interacting with FRP}}{\text{Abudance of monolink for OCP only sample}}$$ (D) An isotope-encoded mass spectrum of crosslinked OCP-FRP showing the K167(OCP)-M1(FRP) cross-link in the orange state is less abundant than in the red state.
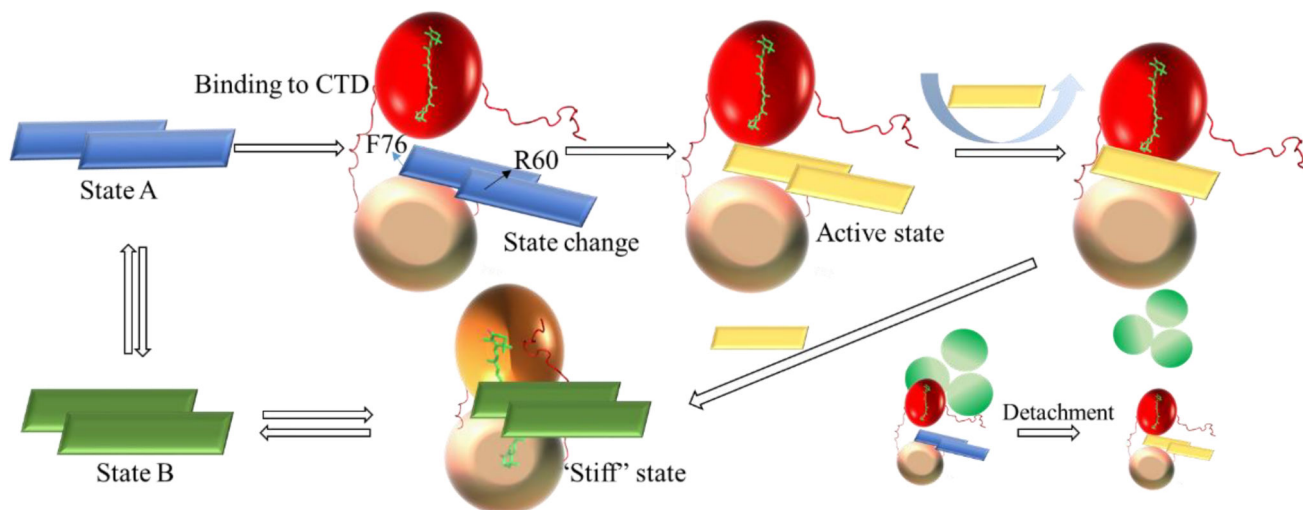
Fig. 9.

Proposed model of the interaction between FRP and OCP. FRP is shown as a rectangle with different colors corresponding to different states; the OCP NTD is shown as a red ball in the red state and an orange ball in the orange state; the OCP CTD is shown as a wheat-colored ball; the APC core from the PBS is shown as three green circles. In the first step, dimeric FRP approaches and binds the CTD, inducing a conformational change in FRP (likely unfolding of the head region) and enabling its binding to the NTD. dFRP forms a stable complex with OCP[r] by bridging the two domains. At the stage, OCP[r] can be detached from PBS by FRP. The cooperative action of the linker region and the N-terminal arm facilitates the dissociation of the FRP dimer. Monomeric FRP is more flexible and effectively facilitates the closing-up of the two OCP domains. Finally, the accelerated conversion process finishes, and dFRP weakly associates with OCP[o] around the linker region. The "capped" N-terminal arm on the CTD inhibits the dFRP from entering the cavity.